

Quantum Phase Transition in the One-Dimensional Extended Quantum Compass Model in a Transverse Field

R. Jafari^{1,2}

¹Research Department, Nanosolar System Company (NSS), Zanjan 45158-65911, Iran*

²Department of Physics, Institute for Advanced Studies in Basic Sciences (IASBS), Zanjan 45137-66731, Iran

(Dated: October 27, 2018)

Quantum phase transitions in the one-dimensional extended quantum compass model in transverse field are studied by using the Jordan-Wigner transformation. This model is always gapful except at the critical surfaces where the energy gap disappears. We obtain the analytic expressions of all critical fields which drive quantum phase transitions. This model shows a rich phase diagram which includes spin-flop, strip antiferromagnetic and saturate ferromagnetic phases in addition to the phase with anti parallel ordering of spin y component on odd bonds. However we study the universality and scaling properties of the transverse susceptibility and nearest-neighbor correlation functions derivatives in different regions to confirm the results obtained using the energy gap analysis.

PACS numbers: 75.10.Jm

I. INTRODUCTION

In the last decade, through the extensive experimental and theoretical works, the role of orbital degree of freedom in determining the magnetic and transport properties of transition-metal oxide materials has been recognized extensively¹⁻³. The complex interplay among the orbital, charge, spin, and lattice degrees of freedom makes their phase diagrams extremely rich and leads various fascinating physical phenomena. For instance, ferroelectricity, colossal magnetoresistance, and charge ordering are the results of the orbital degeneracy in d-shell transition metal oxides⁴.

A simplified model which described the nature of the orbital states in the case of a twofold degeneracy is the Quantum Compass Model (QCM)⁵. First, the model has been used to describe the Mott insulators with orbit degeneracies. It depends on the lattice geometry and belongs to the low energy Hamiltonian originated from the magnetic interactions in Mott-Hubbard systems with the strong spin-orbit coupling⁶. In QCM the orbital degrees of freedom are represented by pseudospin operators and coupled anisotropically in such a way as to mimic the competition between orbital orderings in different directions. For simplicity, the one-dimensional (1D) QCM, is constructed by antiferromagnetic order of X and Y pseudospin components on odd and even bonds, respectively^{7,8}. In addition, the 1D QCM is exactly the same as the 1D reduced Kitaev model⁹. Brzezicki *et al.* obtained an exact solution for the ground-state energy, reveals that the 1D QCM exhibits a first-order transition between two disordered phases with opposite signs of certain local spin correlators. Intriguingly, this first-order transition was found to be accompanied by a diverging correlation length for spin correlations on one sublattice⁷.

Moreover, the extended version of the 1D QCM, obtained by introducing one more tunable parameter, has been studied by Eriksson *et al.*¹⁰. They have identified four distinct ground state phases, are separated by two

intersecting transition lines. One of them defines a line of second-order Ising-like transitions, while the other is a line of first-order transitions. The point of intersection, where the first-order quantum phase transition identified by Brzezicki *et al* takes place, defines a multicritical point. They show that diverging of correlation length for certain spin correlations, has recognized a natural explanation of the multicriticality of the transition point. However, their results for the entanglement show that the only effect on the ground state when going through the first order transitions is that a correlation function for neighboring spins on odd bonds changes sign, without any effect on the entanglement measures. First-order quantum phase transitions (QPT) are generally associated with a discontinuity in concurrence, but accidental exceptions to this rule are possible. To the best of our knowledge, the QCM in a transverse field has not been studied so far, except on the first order transition line¹¹. They have shown that the energy gap does not disappear in the presence of the transverse-field even in the thermodynamic limit.

In this paper, we study the 1D extended quantum compass model (EQCM) in a transverse magnetic field. The exact solution is obtained by using Jordan-Wigner (JW) transformation. We show that this model reveal a rich phase diagram which includes quantum critical surfaces depending on exchange couplings. (We have been made aware that similar work is being performed by M. Motamedifar, S. Mahdaviifar and S. Shayesteh Farjami using the exact diagonalization method, personal communication.) Moreover, as we have shown in our resent work¹², because of nice scaling properties of correlation functions and transverse susceptibility (TS), phase transition can be captured from small systems with considerable accuracy without pre-assumed order parameters even for the cases where the pairwise entanglement is absent. However we have exhibited that the divergence and scaling properties of two-body entanglement could be obtained by studying the correlation functions properties without direct calculation of the entanglement. So we will study

the nearest neighbor correlation (NNC) functions and TS of this model near a quantum critical points (QCP).

II. HAMILTONIAN AND EXACT SOLUTION

Consider the Hamiltonian

$$H = \sum_{n=1}^{N'} [J_1 \sigma_{2n-1}^x \sigma_{2n}^x + J_2 \sigma_{2n-1}^y \sigma_{2n}^y + L_1 \sigma_{2n}^x \sigma_{2n+1}^x + h(\sigma_{2n-1}^z + \sigma_{2n}^z)]. \quad (1)$$

where J_1 and J_2 are the odd bonds exchange couplings, L_1 is the even bond exchange coupling and $N = 2N'$ is the number of spins. We assume periodic boundary conditions. The above Hamiltonian (Eq. (1)) can be exactly diagonalized by standard Jordan-Wigner transformation¹³ as defined below,

$$\sigma_j^x = b_j^+ + b_j^-, \quad \sigma_j^y = b_j^+ - b_j^-, \quad \sigma_j^z = 2b_j^+ b_j^- - 1$$

$$b_j^+ = c_j^\dagger e^{i\pi \sum_{m=1}^{j-1} c_m^\dagger c_m}, \quad b_j^- = e^{-i\pi \sum_{m=1}^{j-1} c_m^\dagger c_m} c_j$$

which transforms spins into fermion operators c_j .

The crucial step is to define independent Majorana fermions¹⁴ at site n , $c_n^q \equiv c_{2n-1}$ and $c_n^p \equiv c_{2n}$. This can be regarded as quasiparticles' spin or as splitting the chain into bi-atomic elementary cells⁸.

Substituting for σ_j^x , σ_j^y and σ_j^z ($j = 2n, 2n-1$) in terms of Majorana fermions with antiperiodic boundary condition (subspace with even number of fermions) followed by a Fourier transformation, Hamiltonian Eq. (1) (apart from additive constant), can be written as

$$H^+ = \sum_k \left[J c_k^{q\dagger} c_{-k}^{p\dagger} + L c_k^{q\dagger} c_k^p + 2h(c_k^{q\dagger} c_k^q + c_k^{p\dagger} c_k^p) + h.c. \right], \quad (2)$$

where $J = (J_1 - J_2) - L_1 e^{ik}$, $L = (J_1 + J_2) + L_1 e^{ik}$ and $k = \pm \frac{j\pi}{N'}$, ($j = 1, 3, \dots, N' - 1$).

It should be pointed out that although the GS in periodic and antiperiodic boundary conditions are slightly different in the finite-size system, they are identical in the thermodynamic limit and the essential features in finite size are also not altered qualitatively.

Finally, diagonalization is completed by a four-dimensional Bogoliubov transformation connecting $c_k^{q\dagger}$, c_{-k}^q , $c_k^{p\dagger}$, c_{-k}^p and obtain two different kind of quasiparticles,

$$H = \sum_k \left[E_k^q (\gamma_k^{q\dagger} \gamma_k^q - \frac{1}{2}) + E_k^p (\gamma_k^{p\dagger} \gamma_k^p - \frac{1}{2}) \right], \quad (3)$$

where $E_k^q = \sqrt{2(a+c)}$ and $E_k^p = \sqrt{2(a-c)}$, $c = \sqrt{a^2 - b}$ in which

$$a = 2h^2 + J_1^2 + J_2^2 + L_1^2 + 2L_1 J_2 \cos k, \\ b = 4[(J_1 J_2 - h^2)^2 + 2J_1 L_2 (J_1 J_2 - h^2) \cos k + J_1^2 L_1^2].$$

The ground state (E_G) and the lowest excited state (E_E) energies are obtained from Eq.(3),

$$E_G = -\frac{1}{2} \sum_k (E_k^q + E_k^p), \quad E_E = -\frac{1}{2} \sum_k (E_k^q - E_k^p),$$

where could be written as a function of a and b ,

$$E_G = -2 \sum_{k>0} \sqrt{a + \sqrt{b}}, \quad E_E = -2 \sum_{k>0} \sqrt{a - \sqrt{b}} \quad (4)$$

It is clear the ground state is separated from the lowest energy pseudospin excitation by a pseudospin gap $\Delta = |E_E - E_G|$, which vanishes at $h_0 = \sqrt{J_1(J_2 + L_1)}$ and $h_\pi = \sqrt{J_1(J_2 - L_1)}$ in the thermodynamic limit.

It should be stressed here that the exact spectrum and the pseudospin gap are the same as that obtained by Eriksson *et al.* for $h = 0$ using a different method¹⁰.

So, the quantum phase transition (QPT) which could be driven by the transverse-field, depending on exchange couplings, occurs at h_0 and h_π .

III. PHASE DIAGRAM

The complete phase diagram of the extended compass model without transverse magnetic field has been reported in Refs. [10] and [15]. They have shown that the first-order transition occurs at multicritical point where a line of first-order transition ($J_1/L_1 = 0$) meets with a line of second order transition ($J_2/L_1 = 1$). Also, There are four gapped phases in the exchange couplings' space,

- (I) $J_1 > 0$, $J_2 < 1$: In this region the ground state is in the Néel phase along the x axis.
- (II) $J_1 > 0$, $J_2 > 1$: In this case there is antiparallel ordering of spin y component on odd bonds.
- (III) $J_1 < 0$, $J_2 > 1$: In this case there is parallel ordering of spin y component on odd bonds.
- (IV) $J_1 < 0$, $J_2 < 1$: In this region the ground state is in the strip antiferromagnetic (SAF) phase.

Phase diagram of extended quantum compass model in transverse field has been shown in Fig. (1). Depending on exchange couplings, the transverse field could drives the phase transition at h_0 and h_π where the energy gap vanishes (For simplicity we take $L_1 = 1$).

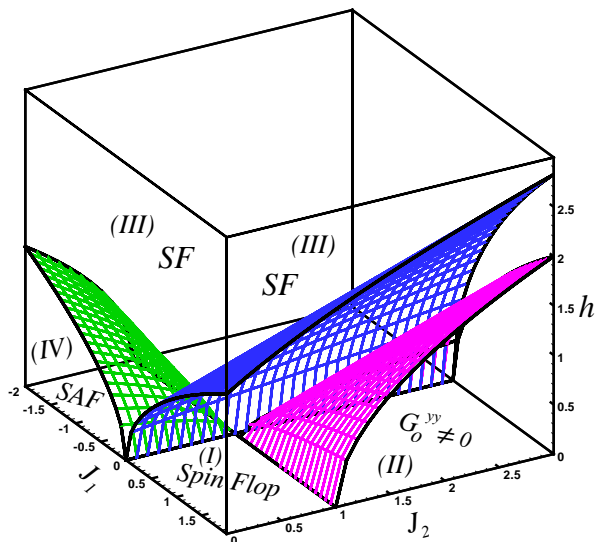


FIG. 1: (Color online) Phase diagram of the extended compass model in the transverse magnetic field. For $J_1 > 0, J_2 < 1$, the front and top side of the purple convex surface is spin-flop phase (I) and the back side ($J_1 > 0, J_2 > 1$) specified by antiparallel ordered of spin y component (II). The blue checkerboard pattern represents the boundary between spin-flop phase (I) and saturate ferromagnetic phase (III). In the case of $J_1 < 0, J_2 < 1$ there are two phases, the strip antiferromagnetic phase (IV) which exists below the green convex surface and the saturate ferromagnetic phase (III) which is above it. For $J_1 < 0, J_2 > 1$ saturate ferromagnetic phase (III) attends the phase diagram. The first-order transition appears just at $J_1 = 0, h = 0$ line.

Fig. (2) shows the absolute value of transverse magnetization (TM) and NNC functions on odd and even bonds for infinite system size in region (I) ($J_1 = 1, J_2 = 0.8$). In this region tuning the magnetic field dictated the system to fall into saturated ferromagnetic (SF) phase. The spin flop-SF phase transition occurs at $h_c = h_0$ (blue checkerboard curved plane in Fig. (1)) which under this surface ground state is in the spin flop phase (the Néel ordered along the axis where is perpendicular to magnetic field is called spin flop). It is seen in Fig. (2) that the onset of magnetic field sets up the TM (M_z) immediately and continuously increases with increase in h to saturate value ($|M_z| = 1$). However, the antiparallel ordered of spin x and y components on odd (G_o^{xx}, G_o^{yy}) and even (G_E^{xx}) bonds reduces by increasing the magnetic field and goes to zero for $h \rightarrow \infty$.

In region (II) the gap decreases by increasing the magnetic field and goes to zero at the lower critical field $h_{c1} = h_\pi$ (purple checkerboard curved plane in Fig. (1)) and beyond this critical field the energy gap immediately appears with increase of the magnetic field. This process continues until the upper critical field $h_{c2} = h_0$ (blue checkerboard curved plane in Fig. (1)) at which the energy gap vanishes and becomes once again gapped upon

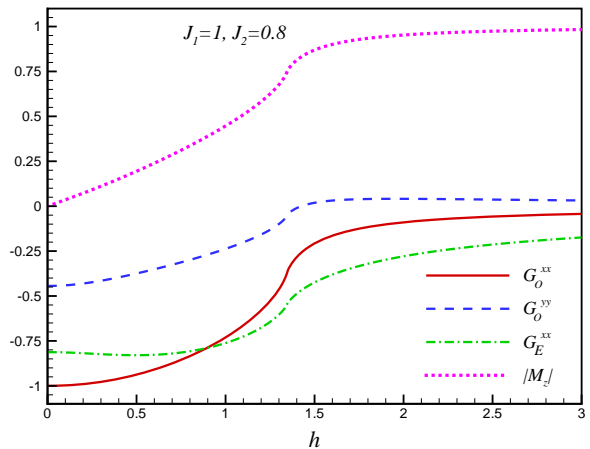


FIG. 2: (Color online) The transverse magnetization and different components of nearest-neighbor spin correlation functions on even and odd bond for $J_1 = 1, J_2 = 0.8$.

the h_{c2} . Fig. (3) shows the TM and NNC functions versus the magnetic field in the region (II) ($J_1 = 1, J_2 = 2$). It manifests that under the lower critical field ($h < h_{c1}$) the antiparallel ordered of spin x and y components on odd and even bonds stay quite unchanged. However the TM is zero for $h < h_{c1}$. So the ground state's antiparallel ordering of spin y component remains unchanged under h_{c1} . Beyond the h_{c1} the TM and NNC functions undergo a strong qualitative change and antiparallel ordered on odd and even bonds tends to zero as the magnetic field increases. Increasing the magnetic field saturates the TM and disappears the antiparallel ordered spin x component on odd bound at $h_{c2} = h_0$, while the antiparallel ordered spin y component on odd bound and antiparallel ordered spin x component on even bond have a nonzero values

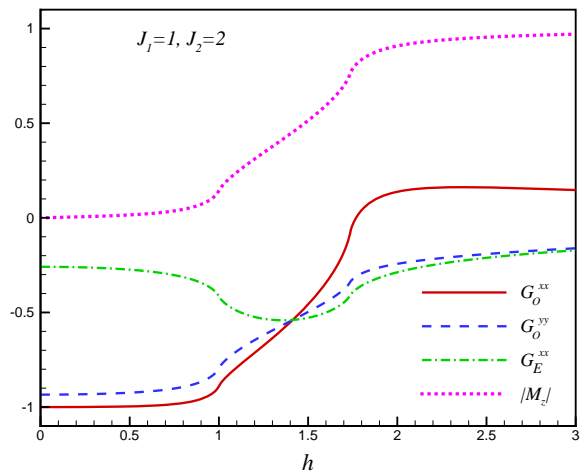


FIG. 3: (Color online) The TM and NNC functions of spin components for $J_1 = 1, J_2 = 2$.

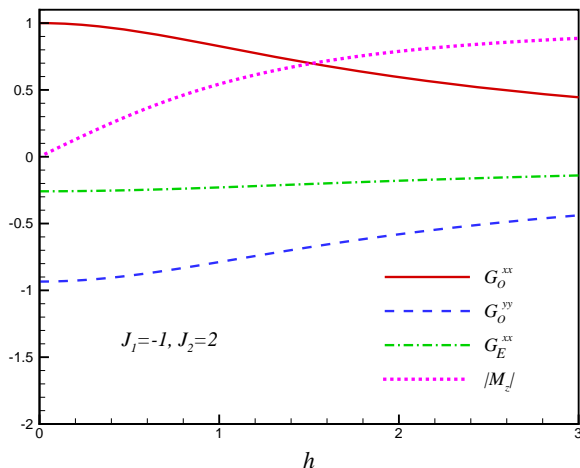


FIG. 4: (Color online) The TM and different components of nearest-neighbor spin correlation functions on even and odd bond in region (III) ($J_1 = -1, J_2 = 2$).

and tend to zero for $h \rightarrow \infty$.

A surprising result occurs in the intermediate region of the magnetic fields $h_{c_1} < h < h_{c_2}$ where increasing the magnetic field enhances the antiparallel ordered spin x component on even bond up to a maximum and then decreases gradually, while decreases the other antiparallel ordered. So we predict that the gapped spin-flop phase exists in the intermediate values of the transverse magnetic field $h_{c_1} < h < h_{c_2}$. In other words, in the region (II), the magnetic field destroys the ground state's antiparallel ordering of spin y component on even bond at h_{c_1} and sticks the system in the spin-flop phase upon the h_{c_1} . The spin-flop-SF transition occurs beyond h_{c_2} .

The TM and NNC functions have been depicted in Fig. (4) for region (III) ($J_1 = -1, J_2 = 2$). In this case the system is in the SF phase and phase transition does not occur by tuning the magnetic field even in the strong magnetic field.

Fig. (5) shows the TM and NNC functions in the region (IV) ($J_1 = -1, J_2 = 0.8$). This region includes two gapped phases, SAF and SF, which are separated from one another at the critical point $h_c = h_\pi$ (green checkerboard curved plane in Fig. (1)).

The three-dimensional panorama of TM with respect to J_2 and h has been plotted in Fig. (6) for $J_1 = 1$. The two critical lines ($h_0(J_2, h)$ and $h_\pi(J_2, h)$) at which the energy gap vanishes can be described by two assumed lines on the two convex parts of the surface in Fig. (5).

IV. UNIVERSALITY AND SCALING OF CORRELATION FUNCTIONS

The nonanalytic behavior in some physical quantity is a feature of second-order quantum phase transition. It is also accompanied by a scaling behavior since the correla-

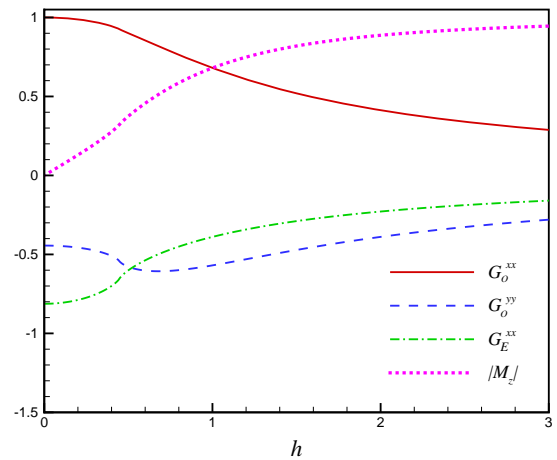


FIG. 5: (Color online) The TM and NNC functions of spin components for $J_1 = -1, J_2 = 0.8$.

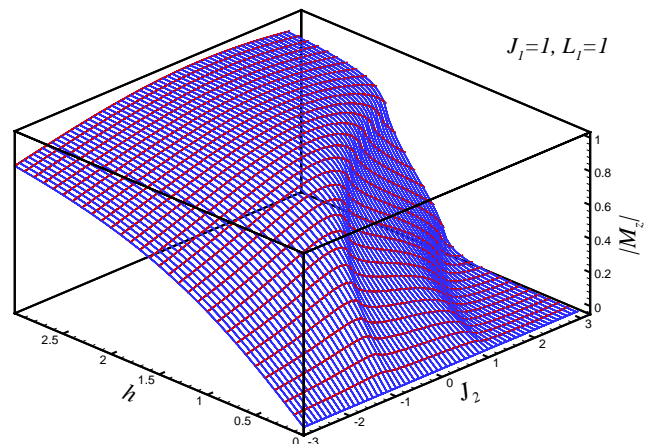


FIG. 6: (Color online) The three-dimensional panorama of TM for $J_1 = 1$.

tion length diverges and there is no characteristic length scale in the system at the critical point. As we previously mentioned, correlation functions and TS show the universality and scaling around the QCP and could capture QCP. However, studying the NNC functions behaviors could reveal the scaling and universality of entanglement near the QCP. So, in this section we will study the behavior of NNC functions derivative with respect to the magnetic field and TS to confirm the previous results.

In Fig. (7) the derivative of G_o^{yy} with respect to the magnetic field has been shown for different system sizes in region (I) ($J_1 = 1, J_2 = 2$). For infinite lattice size dG_o^{yy}/dh diverges as the critical point is touched, while there is no divergence for finite lattice sizes. As the size of system becomes large, the derivative of NNC functions

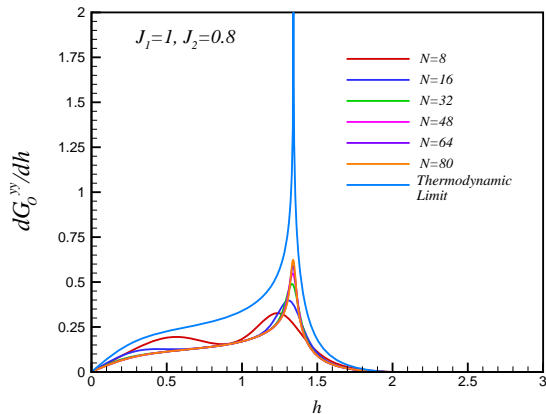


FIG. 7: (Color online) Evolution of the $\frac{dG_o^{yy}}{dh}$ versus h for different system sizes in region (I) for $J_1 = 1, J_2 = 0.8$.

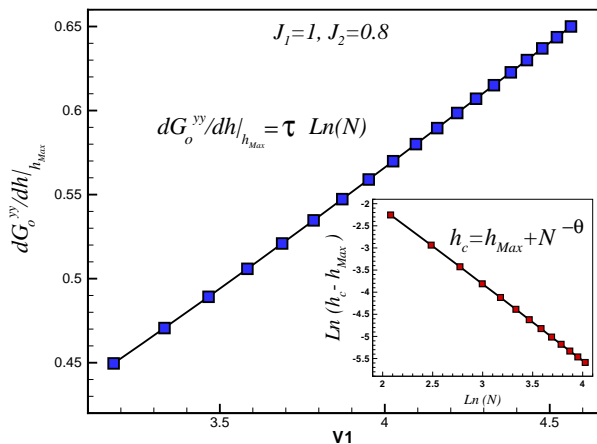


FIG. 8: (Color online) Scaling of the maximum of $\frac{dG_o^{yy}}{dh}$ for systems of various sizes. Inset: Scaling of the position (h_{Max}) of $\frac{dG_o^{yy}}{dh}$ for different-length chains.

tends to diverge close to the critical point. More information can be obtained when the maximum values of each plot and their positions are analyzed. The position of the maximum (h_{Max}) of dG_o^{yy}/dh tends toward the critical point like $h_{Max} = h_c - N^{-\theta}$ ($\theta = 1.72 \pm 0.03$) which has been plotted in the inset of Fig. (8).

Moreover, we have derived the scaling behavior of $|dG_o^{yy}/dh|_{h_{Max}}$ versus N . This has been plotted in Fig. (8) which shows a linear behavior of $|dG_o^{yy}/dh|_{h_{Max}}$ versus $\ln(N)$. The scaling behavior is $|dG_o^{yy}/dh|_{h_{Max}} = \tau \ln(N)$ with $\tau = 0.15 \pm 0.01$. To study the scaling behavior of G_o^{yy} around the critical point, we perform finite-size scaling analysis, since the maximum value of derivative of G_o^{yy} scales logarithmic. According to the scaling ansatz, the rescaled derivative of G_o^{yy} around its maximum value h_{Max} is just a function of rescaled driving parameter such

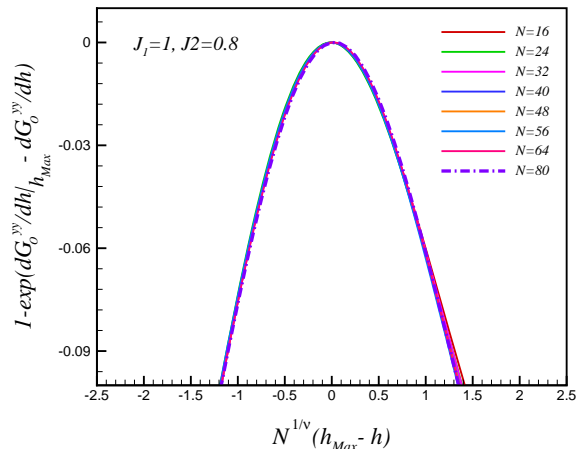


FIG. 9: (Color online) Finite-size scaling of dG_o^{yy}/dh for different lattice sizes. The curves which correspond to different system sizes clearly collapse on a single curve.

as

$$\frac{dG_o^{yy}}{dh} - \frac{dG_o^{yy}}{dh}|_{h_{Max}} \sim F(N^{1/\nu}(h - h_{Max})), \quad (5)$$

where $F(x)$ is a universal function. The manifestation of the finite-size scaling is shown in Fig. (9). It is clear that the different curves which are resemblance of various system sizes collapse to a single universal curve. Our result shows that $\nu = 1 \pm 0.001$ is exactly correspond to the correlation length exponent of Ising model in transverse field ($\nu = 1$).

A similar analysis can be carried on G_o^{xx} , G_E^{xx} and TS (χ^z). Our calculations show that the non-analytic and scaling behavior of NN correlation functions are the same as TS does. It is important to mention that NNC functions and TS show the logarithmic divergence near the QCP. Our results is different from the reported result in Ref. [11]. They have found that TS shows a power-law behavior close to the QCP with the exponent $\gamma = 1.78 \pm 0.05$. Since h is analogous to temperature in classical systems, we expect $h\chi_z$ to be equivalent to the specific heat in the 2D classical Ising model ($J_2 = 0$). So the reported exponent in Ref. [11] belongs to susceptibility in the x -direction not to TS.

We have plotted the derivative of G_o^{yy} in region (II) ($J_1 = 1, J_2 = 2$) versus h in Fig. (10) for different lattice sizes which shows the singular behavior as the size of the system becomes large. As it manifests the divergences of dG_o^{yy}/dh occur at $h_{c1} = 1$ and $h_{c2} = \sqrt{3}$ where exactly correspond to the critical points that obtained using the energy gap analysis ($h_{c1} = h_\pi, h_{c2} = h_0$). A more detailed analysis manifest the linear behavior of $\frac{dG_o^{yy}}{dh}$ at the first maximum point (h_{Max1}) versus $\ln(N)$ where has been plotted in Fig. (11). The exponent for this behavior is $\tau_1 = 0.14 \pm 0.02$.

Moreover, we have shown that the position of the first

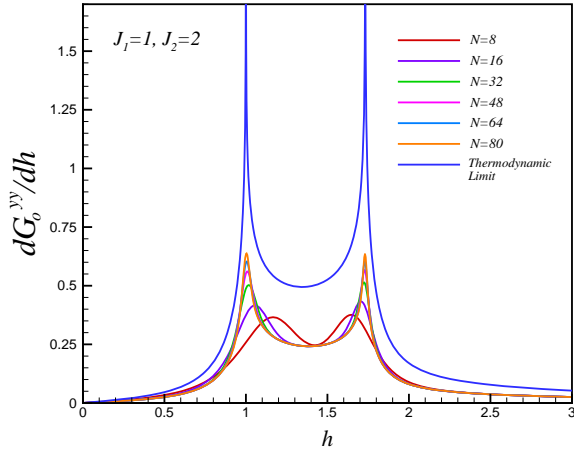


FIG. 10: (Color online) The first order derivative of dG_o^{yy}/dh as a function of h for various system size in region (II) ($J_1 = 1, J_2 = 2$).

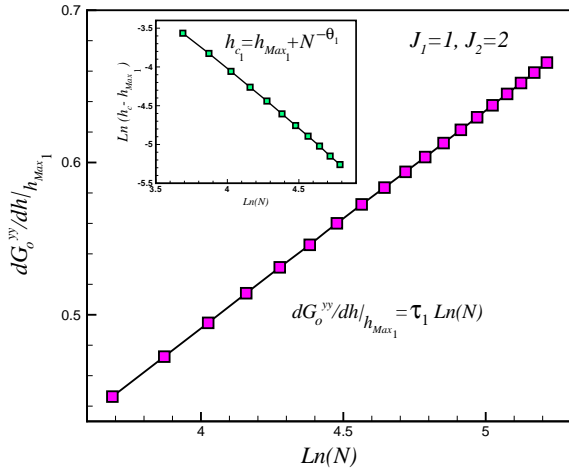


FIG. 11: (Color online) The scaling behavior of the first maximum point of $\frac{dG_o^{yy}}{dh}$ for different-length chain in region (II). Inset: Scaling of the position (h_{Max1}) of $\frac{dG_o^{yy}}{dh}$ for different-length chains ($J_1 = 1, J_2 = 2$).

maximum (h_{Max1}) of dG_o^{yy}/dh goes to the first critical point, such as $h_{Max1} = h_{c1} - N^{-\theta_1}$ with $\theta_1 = 1.59 \pm 0.01$ (Fig. (11, inset)). The similar investigation shows the scaling behavior of $\frac{dG_o^{yy}}{dh}$ at the second maximum point (h_{Max2}) where has been presented in Fig. (12). It specifies a linear behavior of $\frac{dG_o^{yy}}{dh}|_{h_{Max2}}$ versus $\ln(N)$ with the same exponent as $\frac{dG_o^{yy}}{dh}$ treat at the first maximum point ($\tau_2 = 0.14 \pm 0.02$). However, the second maximum position of correlation functions and TS show the scaling behaviors with the same exponents (Fig. (12), inset) as the position of the first maximum of correlation functions and TS do.

We illustrate the finite size scaling behaviors of $\frac{dG_o^{yy}}{dh}$

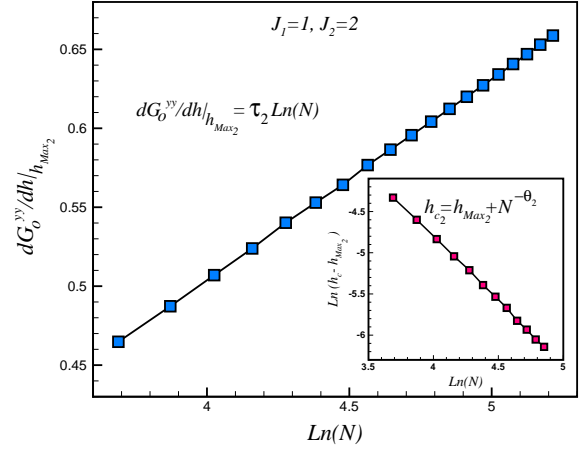


FIG. 12: (Color online) The logarithm of the second maximum of $\frac{dG_o^{yy}}{dh}$ versus the logarithm of chain size, $\ln(N)$, which is linear and shows a scaling behavior ($J_1 = 1, J_2 = 2$). Inset: The scaling behavior of h_{Max2} in terms of system size (N) where h_{Max2} is the position of second maximum in Fig.(10)

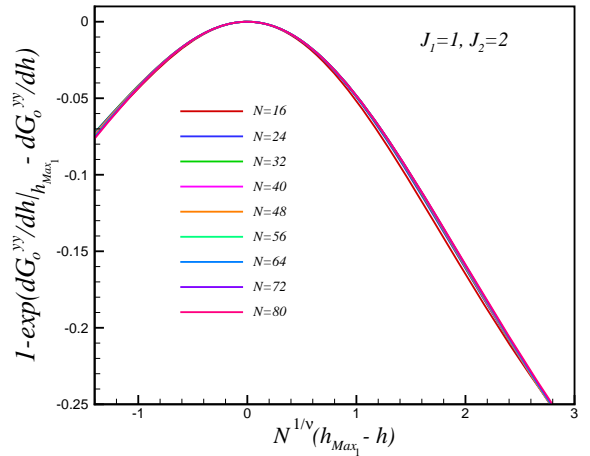


FIG. 13: (Color online) The finite-size scaling analysis for the case of logarithmic divergence around the first maximum point (h_{Max1}) for $J_1 = 1, J_2 = 2$. The NNC function, considered as a function of system size and coupling, collapses on a single curve for different lattice sizes.

around its first and second maximum points in figs. (14) and (15) respectively. They show that the NNC functions can be approximately collapsed to a single curve. These results show that all the key ingredients of the finite size scaling are present in these cases too. In this cases scaling is fulfilled with the critical exponent $\nu = 1$ in agreement with the previous results and universality hypothesis. A similar analysis show that the universality and scaling behavior of G_o^{xx}, G_E^{xx} and TS (χ^z) are the same as each other in region (II).

In Fig. (15) the derivative of G_o^{xx} with respect to mag-

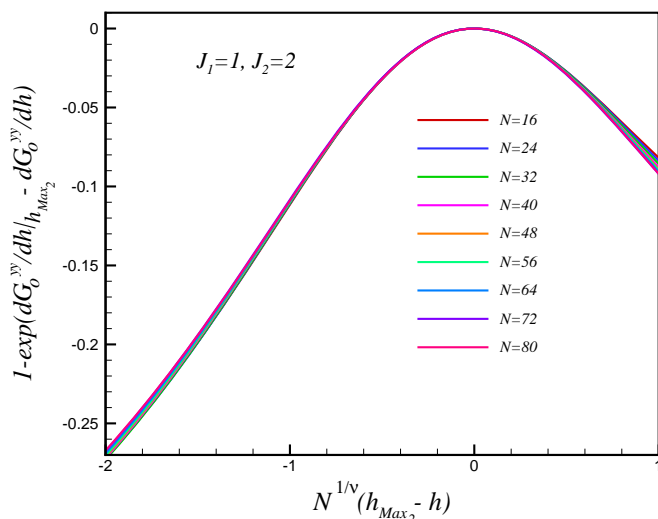


FIG. 14: (Color online) A manifestation of finite-size scaling of $\frac{dG_0^{yy}}{dh}$ around the second maximum point (h_{Max_2}) for various system sizes in region (II).

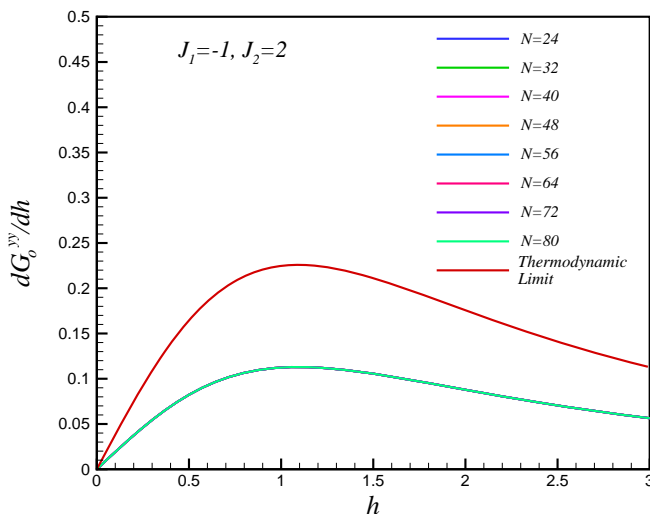


FIG. 15: (Color online) The derivative of dG_0^{yy} versus h in region (III) for $J_1 = -1, J_2 = 2$. Even in the thermodynamic limit no singularity is observed.

netic field has been shown versus h for $J_1 = -1, J_2 = 2$

(region (III)). As it is clear the correlation functions does not show any singularity in this region even at the thermodynamic limit. This is justify our previous finding that shows no transition in this region. We have also investigate the TS and NNC functions behavior in the region (II). Our examination show the logarithmic divergence and scaling behavior of them close to the critical point where has been obtained using the energy gap analysis.

V. SUMMARY AND CONCLUSIONS

In this work we have studied the quantum phase transition in the one-dimensional extended quantum compass model in the presence of a transverse magnetic field. We have shown that there are strip-antiferromagnetic, spin-flop and saturate ferromagnetic phases in addition to the phase with anti parallel ordering of spin y component on odd bonds where phases separated from each other by the critical surfaces. We obtain the analytic expressions of all critical fields for the field-induced quantum phase transitions (QPT). However we have investigate the universality and scaling properties of the nearest neighbor correlation functions and transverse susceptibility to confirm the results were obtained using the energy gap analysis. The results show that the transverse susceptibility and derivatives of the nearest neighbor correlation functions diverge close to the critical point and exhibit beautiful scaling law. So we predict that as the correlation length diverges at the critical point for an infinite system size, the derivative of correlation functions between far neighbors could capture the quantum critical point too. The obtained exponents ($\nu = 1$) and universality behaviors (logarithmic divergence) are nearly the same as those in the 1D transverse-field Ising model¹², suggesting that these two models share the same universality class.

Further investigations including blocks and multi-body correlations functions and the effect of temperature may be interesting to establish a precise comparison between universality and scaling behaviors of correlation functions and entanglement at critical points. Moreover, dynamics of correlation functions may also provide an interesting scenario for the discussion of the properties of the correlation functions and its implications for phase transitions. Such topics are left for a future research.

References

-
- * jafari@iasbs.ac.ir, jafari@nss.co.ir
 - ¹ J. B. Goodenough, Phys. Rev. **100**, 564 (1955).
 - ² Y. Tokura and N. Nagaosa, Science **288**, 462 (2000).
 - ³ Y. Wakabayashi, D. Bizen, H. Nakao, Y. Murakami, M. Nakamura, Y. Ogimoto, K. Miyano, and H. Sawa, Phys. Rev. Lett. **96**, 017202 (2006).
 - ⁴ S.W. Cheong, Nature Mater. **6**, 927 (2007).
 - ⁵ K. I. Kugel and D. I. Khomskii, Sov. Phys. JETP **37**, 725 (1973).
 - ⁶ G. Jackeli and G. Khaliullin, Phys. Rev. Lett. **102**, 017205 (2009).
 - ⁷ W. Brzezicki, J. Dziarmaga, and A. M. Oleś, Phys. Rev.

- B **75**, 134415 (2007).
- ⁸ W. Brzezicki, J. Dziarmaga, and A. M. Oleś, *Acta Phys. Pol. A* **115**, 162 (2009).
- ⁹ X. Y. Feng, G. M. Zhang, and T. Xiang, *Phys. Rev. Lett.* **98**, 087204 (2007).
- ¹⁰ Erik Eriksson and Henrik Johannesson, *Phys. Rev. B* **79**, 224424 (2009).
- ¹¹ Ke-Wei Sun and Qing-Hu Chen, *Phys. Rev. B* **80**, 174417 (2009).
- ¹² R. Jafari, e-print arXiv:1101.2354v1.
- ¹³ E. Lieb, T. Schultz, and D. Mattis, *Ann. Phys. (N.Y.)* **16**, 407 (1961); E. Barouch and B. M. McCoy, *Phys. Rev. A* **3**, 786 (1971); J. B. Kogut, *Rev. Mod. Phys.* **51**, 659 (1979); J. E. Bunder and R. H. McKenzie, *Phys. Rev. B* **60**, 344 (1999).
- ¹⁴ K. Sengupta, D. Sen, and S. Mondal, *Phys. Rev. Lett.* **100**, 077204 (2008); S. Mondal, D. Sen, and K. Sengupta, *Phys. Rev. B* **78**, 045101 (2008).
- ¹⁵ S. MahdaviFar, *Eur. Phys. J. B* **77**, 77-82 (2010).